



UNIVERSITÀ  
DEGLI STUDI  
DI UDINE

## Università degli studi di Udine

Equations with infinite delay: Numerical bifurcation analysis via  
pseudospectral discretization

*Original*

*Availability:*

This version is available <http://hdl.handle.net/11390/1143571.7> since 2021-03-18T14:21:40Z

*Publisher:*

*Published*

DOI:10.1016/j.amc.2018.03.104

*Terms of use:*

The institutional repository of the University of Udine (<http://air.uniud.it>) is provided by ARIC services. The aim is to enable open access to all the world.

*Publisher copyright*

(Article begins on next page)

# Equations with infinite delay: numerical bifurcation analysis via pseudospectral discretization

Mats Gyllenberg<sup>a</sup>, Francesca Scarabel<sup>a</sup>, Rossana Vermiglio<sup>b</sup>

<sup>a</sup>*Department of Mathematics and Statistics, University of Helsinki, P.O. Box 68  
(Gustaf H  llstr  min katu 2b), FI-00014 Helsinki, Finland*

<sup>b</sup>*Department of Mathematics, Computer Science and Physics, University of Udine,  
via delle Scienze 206, I-33100 Udine, Italy*

---

## Abstract

We address the problem of the numerical bifurcation analysis of general nonlinear delay equations, including integral and integro-differential equations, for which no software is currently available. The pseudospectral discretization is applied to the abstract reformulation of equations with infinite delay to obtain a finite dimensional system of ordinary differential equations, whose properties can be numerically studied with the well-developed software. We explore the applicability of the method on some test models and provide some numerical evidence of the convergence of the approximations.

*Keywords:* Volterra integral equations, renewal equations, delay differential equations, Laguerre pseudospectral discretization, physiologically structured population models, finite dimensional state representation, infinite delay

*2010 MSC:* 34K99, 37M20, 65J08, 65L07, 65P30, 92D25

---

## 1. Introduction

Delay equations, including integral and integro-differential equations, play a fundamental role in mathematical models arising from different research fields, going from engineering to physics and biology, because they allow to incorporate “memory” into the model and to describe the effects of past events on the present time.

A specific application that we have in mind comes from ecological models of physiologically structured populations. These models can often be formulated as systems where a nonlinear renewal equation describing the evolution of the total population birth rate is coupled with a delay differential equation describing the evolution of the environmental feedback variable, see for instance [20, 30] and references therein. Also a large class of epidemiological models can be formulated as a nonlinear renewal equation for the force of infection [3, 33, 35].

In many contexts, including the biological applications mentioned above, the investigation focuses not on the solution of the initial value problem associated to the system,

---

\*Corresponding author

Email address: francesca.scarabel@helsinki.fi (Francesca Scarabel)

Preprint submitted to Applied Mathematics and Computation

April 7, 2017

but rather on its long-term dynamics, including for instance equilibria, periodic solutions, and chaotic behavior. This explains the importance of *bifurcation analysis*, viz., the study of how the dynamical properties of a system change under the variation of model parameters.

The infinite-dimensionality and complexity of models with delay, especially in presence of nonlinear equations, make it usually impossible to investigate their properties analytically. Instead, one has to rely on suitable numerical methods. For specific types of equations, namely delay differential equations with discrete delays, the bifurcation analysis can be performed with *ad hoc* numerical packages like, for instance, DDE-BIFTOOL [23], KNUT [40] or XPP [24]. For specific models of physiologically structured populations of the type described above, some free software allows to perform the numerical analysis of equilibria, including their continuation with respect to one parameter, the computation of stability, and the analysis of evolutionary dynamics [15]. Moreover, some MATLAB codes are available for the stability analysis of equilibria and periodic solutions of linear delay equations [6, 7, 9]. But, to our knowledge, no software is currently available for the numerical bifurcation analysis of general nonlinear delay equations like, for instance, systems where a renewal equation is coupled with a delay differential equation.

In [4] the authors proposed a new perspective on the numerical bifurcation analysis of nonlinear equations with finite delay by deriving a finite dimensional system of Ordinary Differential Equations (ODEs) through the pseudospectral discretization approach. The dynamics of the original system can be approximated by means of well-established software for the bifurcation analysis of ODEs, for instance AUTO [22] or MATCONT [17, 28], with no need of developing specific software for delay equations, see also [5] for an application. The technique presented in [4] is based on the reformulation of the delay equation as an Abstract Differential Equation (ADE). However, it restricts to the case of finite maximal delay, although in many cases it is not possible, or not desirable, to bound the maximal delay *a priori*. The aim of this paper is to extend the approach to equations with infinite delay: like in the case of finite delay, the approximating finite dimensional system of ODEs can be studied numerically with available software for ODEs, which, as further advantage, is widely developed and allows for an advanced bifurcation analysis that includes, among others, bifurcations of equilibria and cycles, continuation of homoclinic orbits and computation of normal forms.

To validate the approach, we will explore numerically its applicability and effectiveness on some examples. With this purpose in mind, models coming from biological applications provide particularly suitable test examples because in some cases they can be equivalently formulated as systems of ODEs, following a procedure used already in [29] and presented in [36] as “linear chain trick.” Recently, conditions under which a nonlinear delay model can be reduced to a system of ODEs have been studied in [19, 31] with special attention to applications to physiologically structured populations. The same technique has also been exploited in the context of epidemiological models, see, e.g., [35]. The representation of a system with infinite delay as an equivalent system of ODEs provides a useful way to test quantitatively the numerical results obtained via the proposed approximation technique.

The paper is organized as follows. In Section 2 we recall the basic definitions and results on equations with infinite delay from the point of view of dynamical systems. In Section 3 we describe the discretization approach: we approximate the state of the system with an interpolating polynomial and we apply the collocation technique to a suitable

ADE. This approach returns a finite dimensional system of ODEs approximating the original equation. In Section 4 we test the method for the bifurcation analysis of some test models, providing numerical evidence of the accuracy of the approximation.

## 2. Equations with infinite delay

Consider the system of delay equations

$$\begin{cases} x(t) = F(x_t, y_t) \\ \frac{dy}{dt}(t) = G(x_t, y_t), \end{cases} \quad t > 0, \quad (1)$$

for  $x(t) \in \mathbb{R}^{d_X}$ ,  $y(t) \in \mathbb{R}^{d_Y}$ , with  $d_X, d_Y \in \mathbb{N}$ . The subscript  $t$  is a standard notation to indicate the history of a given function up to time  $t$ : for all  $t \geq 0$ ,  $z_t$  is defined by

$$z_t(\theta) := z(t + \theta), \quad \theta \leq 0.$$

In the biological applications that we mainly consider, the first equation is usually a Volterra integral equation, also referred to as a (nonlinear) renewal equation.

Let  $\rho > 0$  be a scaling parameter such that  $F$  and  $G$  are continuous and sufficiently smooth functions defined on the product space  $X_\rho \times Y_\rho$ , where  $X_\rho$ ,  $Y_\rho$  are spaces of functions defined by

$$\begin{aligned} X_\rho &:= L_\rho^1(\mathbb{R}_-, \mathbb{R}^{d_X}) = \{\varphi: \mathbb{R}_- \rightarrow \mathbb{R}^{d_X} \mid \varphi \text{ measurable, } \int_{-\infty}^0 e^{\rho\theta} |\varphi(\theta)| d\theta < \infty\} \\ Y_\rho &:= C_{0,\rho}(\mathbb{R}_-, \mathbb{R}^{d_Y}) = \{\psi: \mathbb{R}_- \rightarrow \mathbb{R}^{d_Y} \mid \psi \text{ continuous, } \lim_{\theta \rightarrow -\infty} e^{\rho\theta} \psi(\theta) = 0\}. \end{aligned}$$

Here  $|\cdot|$  is a norm in  $\mathbb{R}^{d_X}$  or  $\mathbb{R}^{d_Y}$  depending on the context.  $(X_\rho, \|\cdot\|_{1,\rho})$  and  $(Y_\rho, \|\cdot\|_{\infty,\rho})$  are Banach spaces with the weighted norms

$$\begin{aligned} \|\varphi\|_{1,\rho} &:= \int_{-\infty}^0 e^{\rho\theta} |\varphi(\theta)| d\theta \\ \|\psi\|_{\infty,\rho} &:= \sup_{\theta \leq 0} e^{\rho\theta} |\psi(\theta)|. \end{aligned}$$

Notice that, given  $0 < \rho < \bar{\rho}$ , the norms satisfy

$$\begin{aligned} \|\varphi\|_{1,\bar{\rho}} &\leq \|\varphi\|_{1,\rho}, \quad \varphi \in L_\rho^1(\mathbb{R}_-, \mathbb{R}^d) \\ \|\psi\|_{\infty,\bar{\rho}} &\leq \|\psi\|_{\infty,\rho}, \quad \psi \in C_{0,\rho}(\mathbb{R}_-, \mathbb{R}^d), \end{aligned}$$

and the following inclusions hold:

$$\begin{aligned} L_\rho^1(\mathbb{R}_-, \mathbb{R}^d) &\subset L_{\bar{\rho}}^1(\mathbb{R}_-, \mathbb{R}^d) \\ C_{0,\rho}(\mathbb{R}_-, \mathbb{R}^d) &\subset C_{0,\bar{\rho}}(\mathbb{R}_-, \mathbb{R}^d). \end{aligned}$$

Given  $\varphi \in X_\rho$  and  $\psi \in Y_\rho$ , a *solution* of (1) with initial condition

$$\begin{cases} x(\theta) = \varphi(\theta) \\ y(\theta) = \psi(\theta), \end{cases} \quad \theta \leq 0, \quad (2)$$

is a couple  $(x, y)$  defined on  $(-\infty, t_f]$ ,  $t_f > 0$ , such that for all  $t \in (-\infty, t_f]$  one has  $x_t \in X_\rho$ ,  $y_t \in Y_\rho$ , and  $(x, y)$  satisfies (1) and (2) (see, for instance, [21, 32]). The choice of the space of integrable functions is motivated by the fact that the solution  $x$  may be discontinuous in  $t = 0$  and by the interpretation in the context of models from ecology, where the variable  $x$  usually denotes a rate. Notice, however, that for  $t > 0$  the solution  $x$  is defined pointwise, and not just almost everywhere. Moreover, if  $F$  is continuous, so is  $x$  for  $t > 0$ . One reason for choosing the weighted norm is that we want constant functions to belong to the state space.

Equations (1)–(2) define a dynamical system on the space  $X_\rho \times Y_\rho$ , where the semi-group of solution operators  $\mathcal{S} = \{S(t)\}_{t \geq 0}$  is defined by

$$\begin{aligned} S(t): X_\rho \times Y_\rho &\rightarrow X_\rho \times Y_\rho \\ (\varphi, \psi) &\mapsto (x_t, y_t). \end{aligned}$$

The infinitesimal generator of  $\mathcal{S}$  is the operator  $\mathcal{A}: D(\mathcal{A}) (\subseteq X_\rho \times Y_\rho) \rightarrow X_\rho \times Y_\rho$  such that

$$\mathcal{A}(\varphi, \psi) = (\varphi', \psi'), \quad (\varphi, \psi) \in D(\mathcal{A}) \quad (3)$$

$$D(\mathcal{A}) = \left\{ (\varphi, \psi) \in X_\rho \times Y_\rho \mid (\varphi', \psi') \in X_\rho \times Y_\rho \text{ and } \begin{cases} \varphi(0) = F(\varphi, \psi) \\ \psi'(0) = G(\varphi, \psi) \end{cases} \right\}, \quad (4)$$

see [13, 14], where we use  $(\varphi', \psi') \in X_\rho \times Y_\rho$  as a shorthand notation to indicate that  $\varphi \in X_\rho$ ,  $\varphi$  is absolutely continuous with  $\varphi = \int \eta(\theta) d\theta$ ,  $\eta \in X_\rho$ , and  $\psi \in Y_\rho$  is continuously differentiable with  $\psi' \in Y_\rho$ . To avoid overloading the notation, we write  $\mathcal{A}(\varphi, \psi)$  instead of  $\mathcal{A}((\varphi, \psi))$ . Notice that the action of  $\mathcal{A}$  is linear and the nonlinearity of  $\mathcal{A}$  stems from the fact that the domain  $D(\mathcal{A})$  is not a linear subspace. By means of the operator  $\mathcal{A}$  we can define the ADE

$$\frac{d}{dt}(u(t), v(t)) = \mathcal{A}(u(t), v(t)), \quad t > 0, \quad (5)$$

for  $(u(t), v(t)) \in X_\rho \times Y_\rho$ . The ADE (5) together with the initial condition

$$(u(0), v(0)) = (\varphi, \psi) \quad (6)$$

is equivalent to (1)–(2) in the sense that every solution  $x(t) \in \mathbb{R}^{d_x}$ ,  $y(t) \in \mathbb{R}^{d_y}$  of (1) with initial condition (2) defines a weak solution  $u(t) := x_t \in X_\rho$ ,  $v(t) := y_t \in Y_\rho$  of (5)–(6) for all  $t \geq 0$  and vice versa, see [18] for details.

We are interested in the asymptotic behavior of the solutions of (1)–(2), and in particular in the stability properties of equilibria and periodic solutions. An important tool in the investigation of stability is the *principle of linearized stability*, that characterizes the local stability properties of a solution  $(x, y)$  of (1) in terms of the stability of the zero solution of the system linearized at  $(x, y)$ . While no general theory about linearization at a periodic solution, like the Floquet theory for ODEs, has been developed yet in the general case (but see [21] for the treatment of delay differential equations with finite delay), the principle of linearized stability for equilibria of systems of type (1) with infinite delay has been proved in [18] using a modification of the sun-star calculus developed in [10–12, 21]. We recall here the main details that will be useful later on in the discretization procedure.

We recall that an *equilibrium* of (1) is a constant solution  $\bar{x}(t) = \bar{x} \in \mathbb{R}^{d_x}$ ,  $\bar{y}(t) = \bar{y} \in \mathbb{R}^{d_y}$ ,  $t \in \mathbb{R}$ , such that

$$\begin{cases} \bar{x} = F(\bar{x}, \bar{y}) \\ 0 = G(\bar{x}, \bar{y}). \end{cases} \quad (7)$$

The linearization of (1) at  $(\bar{x}, \bar{y})$  is the linear system

$$\begin{cases} x(t) = D_x F(\bar{x}, \bar{y})x_t + D_y F(\bar{x}, \bar{y})y_t \\ \frac{dy}{dt}(t) = D_x G(\bar{x}, \bar{y})x_t + D_y G(\bar{x}, \bar{y})y_t, \end{cases} \quad t > 0,$$

where  $DF = (D_x F, D_y F)$  and  $DG = (D_x G, D_y G)$  denote the Fréchet derivative of  $F$  and  $G$ , respectively. The Riesz representation theorem ensures that the linearized system can be written as

$$\begin{cases} x(t) = \int_0^{+\infty} k_{11}(s)x(t-s)ds + \int_{\mathbb{R}_+} \mu_{12}(ds)y(t-s) \\ \frac{dy}{dt}(t) = \int_0^{+\infty} k_{21}(s)x(t-s)ds + \int_{\mathbb{R}_+} \mu_{22}(ds)y(t-s), \end{cases} \quad t > 0, \quad (8)$$

where, for  $j = 1, 2$ ,

$$\begin{aligned} \sup_{s \geq 0} e^{-\rho s} |k_{j1}(s)| &< \infty, \\ \int_{\mathbb{R}_+} e^{-\rho s} |\mu_{j2}(ds)| &< \infty. \end{aligned}$$

In other words, the entries of  $k_{j1}$  are elements of the dual space  $X_\rho^*$ , while the entries of  $\mu_{j2}$  are elements of the dual space  $Y_\rho^*$ . Notice that the matrices  $k_{11}$  and  $\mu_{12}$  map into the space  $\mathbb{R}^{d_x}$ , while  $k_{21}$  and  $\mu_{22}$  map into the space  $\mathbb{R}^{d_y}$ . In fact, the kernels  $k_{j1}$  have additional regularity properties, as guaranteed by the following result, which we restate here for convenience.

**Theorem 1** ([18], Corollary 3.2). *Let  $0 < \rho < \bar{\rho}$  and  $d \in \mathbb{N}$ . Let  $H: X_{\bar{\rho}} \times Y_{\bar{\rho}} \rightarrow \mathbb{R}^d$  be Fréchet differentiable at  $(\varphi, \psi) \in X_\rho \times Y_\rho \subset X_{\bar{\rho}} \times Y_{\bar{\rho}}$  with Fréchet derivative  $DH(\varphi, \psi)$  represented by a kernel  $(k, \mu)$ . Then  $H$  is Fréchet differentiable at  $(\varphi, \psi)$  as a function from  $X_\rho \times Y_\rho$  into  $\mathbb{R}^d$ . Its Fréchet derivative is represented by  $(k, \mu)$  and  $k$  belongs not only to  $L_\rho^\infty(\mathbb{R}_+, \mathbb{R}^{d \times d})$  but also to  $L_\rho^1(\mathbb{R}_+, \mathbb{R}^{d \times d})$ .*

From now on, we will assume that  $\rho$  is chosen such that  $k_{11} \in L_\rho^1(\mathbb{R}_+, \mathbb{R}^{d_x \times d_x})$  and  $k_{21} \in L_\rho^1(\mathbb{R}_+, \mathbb{R}^{d_y \times d_x})$ . Notice that, if  $(\varphi, \psi)$  is bounded (as, for instance, for equilibria and periodic solutions), then  $(\varphi, \psi) \in X_\rho \times Y_\rho$  for any  $\rho > 0$ . Hence, if  $F$  and  $G$  are defined on the maximal space  $X_{\bar{\rho}} \times Y_{\bar{\rho}}$ , the linearization (8) at  $(\varphi, \psi)$  can be interpreted as a dynamical system on the smaller state space  $X_\rho \times Y_\rho$ . This ensures some flexibility in the choice of the state space  $X_\rho \times Y_\rho$  that we will exploit in the numerical computations to select the parameter  $\rho$  which improves the efficiency of the numerical scheme.

Let  $\{T(t)\}_{t \geq 0}$  be the linear semigroup associated to (8) and let  $\mathcal{A}$  be its infinitesimal generator. In [18] it was proved that every element  $\lambda$  of the spectrum of  $\mathcal{A}$  belonging to the right half-plane

$$\mathbb{C}_\rho := \{\lambda \in \mathbb{C} : \Re(\lambda) > -\rho\}$$

is an eigenvalue and satisfies the characteristic equation

$$\det \mathcal{M}(\lambda) = 0 \quad (9)$$

with

$$\mathcal{M}(\lambda) := \begin{pmatrix} I_{d_X} & 0 \\ 0 & \lambda I_{d_Y} \end{pmatrix} - \begin{pmatrix} \mathcal{L}(k_{11})(\lambda) & \mathcal{L}(\mu_{12})(\lambda) \\ \mathcal{L}(k_{21})(\lambda) & \mathcal{L}(\mu_{22})(\lambda) \end{pmatrix},$$

where  $\mathcal{L}(\cdot)$  denotes the Laplace transform of a function or the Laplace–Stieltjes transform of a measure. The eigenfunctions  $(\varphi, \psi)$  corresponding to  $\lambda$  have the form

$$(\varphi(\theta), \psi(\theta)) = (c_1, c_2)e^{\lambda\theta}, \quad \theta \leq 0,$$

for some  $c_1 \in \mathbb{C}^{d_X}$ ,  $c_2 \in \mathbb{C}^{d_Y}$ , not both zero. Moreover, there are finitely many roots of (9) in  $\mathbb{C}_\rho$ . This allows to prove the principle of linearized stability, which we restate here for convenience.

**Theorem 2** ([18], Principle of linearized stability). *Assume that  $F$  and  $G$  are continuously Fréchet differentiable. Let  $(\bar{x}, \bar{y})$  be an equilibrium of (1) and let (8) be the linearization of (1) at  $(\bar{x}, \bar{y})$ .*

- (a) *If all the roots of the characteristic equation (9) have negative real part, then  $(\bar{x}, \bar{y})$  is exponentially stable.*
- (b) *If there exists at least one root of (9) with positive real part, then  $(\bar{x}, \bar{y})$  is unstable.*

Motivated by the theoretical results and in line with the case of finite delay [9], a satisfactory discretization procedure should provide, when applied to linear equations, a good approximation of the eigenvalues of  $\mathcal{A}$  which lie in the half-plane  $\mathbb{C}_\rho$ , possibly neglecting the part of the spectrum in  $\mathbb{C} \setminus \mathbb{C}_\rho$ .

### 3. Pseudospectral discretization approach

Consider the system of nonlinear equations (1) and the equivalent ADE (5). We now assume that  $\rho > 0$  is fixed. Since no confusion arises, we drop the subscript  $\rho$  and denote the state space simply as  $X \times Y$ . In analogy with the pseudospectral discretization of equations with finite delay described in [4], our aim is to approximate the nonlinear operator  $\mathcal{A}$  defined in (3)–(4) with a finite dimensional operator acting on a finite dimensional subspace  $X_M \times Y_M \subset X \times Y$ . The following result motivates the choice of  $X_M$  and  $Y_M$  as the spaces of polynomials of degree  $M$ , since it ensures that they are dense in the space of continuous functions, and hence it can be exploited in the approximation of functions  $(\varphi, \psi) \in D(\mathcal{A})$ .

**Theorem 3** ([25], Theorem 6.1.4). *Let  $\rho > 0$  and  $\psi \in C_{0,\rho}(\mathbb{R}_-, \mathbb{R})$ . Then, for any  $\varepsilon > 0$  we can find  $M \in \mathbb{N}$  and a polynomial  $p_M$ , of degree less than or equal to  $M$ , such that for all  $\theta \leq 0$*

$$|\psi(\theta) - p_M(\theta)|e^{\rho\theta} < \varepsilon.$$

In practice, computations with polynomials on the unbounded domain  $\mathbb{R}_-$  can lead to unstable algorithms. Consequently, in order to have reliable implementations it is recommended to work with weighted polynomials and functions vanishing at  $-\infty$ , see for instance [2, 25, 38, 39]. For this reason, in the next sections we project the ADE (5) into a suitable subspace of  $L^1(\mathbb{R}_-, \mathbb{R}^{d_X}) \times C_0(\mathbb{R}_-, \mathbb{R}^{d_Y})$ .

### 3.1. Projection into the space of weighted functions

To simplify the notation, we denote  $w(\theta) = e^{\rho\theta}$  and, for a given space of functions  $\mathcal{F}$ , we call the space of weighted functions of  $\mathcal{F}$  as

$$w\mathcal{F} := \{\hat{\varphi} \mid \hat{\varphi} = w\varphi, \varphi \in \mathcal{F}\}.$$

Let  $\hat{X} := wX \subseteq L^1(\mathbb{R}_-, \mathbb{R}^{d_x})$  and  $\hat{Y} := wY \subseteq C_0(\mathbb{R}_-, \mathbb{R}^{d_y})$  be the spaces of weighted functions of  $X$  and  $Y$  respectively, so that  $\hat{X}$  and  $\hat{Y}$  contain (equivalence classes of) functions that vanish at  $-\infty$ .

Multiplication with the weight function  $w$  defines the transformation

$$\begin{aligned} \hat{\cdot} : X \times Y &\rightarrow \hat{X} \times \hat{Y} \\ (\varphi, \psi) &\mapsto (\hat{\varphi}, \hat{\psi}) := (w\varphi, w\psi). \end{aligned} \tag{10}$$

Notice that, for any function  $\varphi$  defined on  $\mathbb{R}_-$ , we have  $\hat{\varphi}(0) = \varphi(0)$  and

$$w\varphi' = \hat{\varphi}' - \frac{w'}{w}\hat{\varphi} = \hat{\varphi}' - \rho\hat{\varphi}.$$

Let  $\mathcal{A}$  be the operator (3)–(4). We introduce the functions  $\hat{F}, \hat{G}$  defined on  $\hat{X} \times \hat{Y}$  with values in  $\mathbb{R}^{d_x}$  and  $\mathbb{R}^{d_y}$  respectively, such that

$$\begin{aligned} \hat{F}(\hat{\varphi}, \hat{\psi}) &:= F(\hat{\varphi}/w, \hat{\psi}/w) \\ \hat{G}(\hat{\varphi}, \hat{\psi}) &:= G(\hat{\varphi}/w, \hat{\psi}/w), \end{aligned}$$

and the operator  $\hat{\mathcal{A}}: D(\hat{\mathcal{A}})(\subseteq \hat{X} \times \hat{Y}) \rightarrow \hat{X} \times \hat{Y}$  such that

$$\hat{\mathcal{A}}(\hat{\varphi}, \hat{\psi}) = (\hat{\varphi}' - \rho\hat{\varphi}, \hat{\psi}' - \rho\hat{\psi}), \quad (\hat{\varphi}, \hat{\psi}) \in D(\hat{\mathcal{A}}) \tag{11}$$

$$D(\hat{\mathcal{A}}) = \left\{ (\hat{\varphi}, \hat{\psi}) \in \hat{X} \times \hat{Y} \mid (\hat{\varphi}', \hat{\psi}') \in \hat{X} \times \hat{Y} \text{ and } \begin{cases} \hat{\varphi}(0) = \hat{F}(\hat{\varphi}, \hat{\psi}) \\ \hat{\psi}'(0) - \rho\hat{\psi}(0) = \hat{G}(\hat{\varphi}, \hat{\psi}) \end{cases} \right\}. \tag{12}$$

It is easy to show that, defining  $\hat{u}(t) := wu(t)$  and  $\hat{v}(t) := wv(t)$  for all  $t \geq 0$ , the ADE (5) is equivalent to the following ADE in the space  $\hat{X} \times \hat{Y}$

$$\frac{d}{dt}(\hat{u}(t), \hat{v}(t)) = \hat{\mathcal{A}}(\hat{u}(t), \hat{v}(t)), \quad t > 0. \tag{13}$$

For linear systems (8), the linear operators  $\mathcal{A}$  and  $\hat{\mathcal{A}}$  have the same eigenvalues in  $\mathbb{C}_\rho$  and the eigenfunctions associated to an eigenvalue  $\lambda$  are in one-to-one correspondence according to the transformation (10). Indeed, by imposing the domain conditions (4) and (12) it is easy to verify that the eigenvalues  $\lambda$  satisfy the same characteristic equation (9) and the eigenfunctions of  $\hat{\mathcal{A}}$  are  $(\hat{\varphi}, \hat{\psi})$  with

$$(\hat{\varphi}(\theta), \hat{\psi}(\theta)) = (c_1, c_2)e^{(\lambda+\rho)\theta}, \quad \theta \leq 0,$$

for  $c_1 \in \mathbb{C}^{d_x}$ ,  $c_2 \in \mathbb{C}^{d_y}$ , not both zero.



### 3.2. Pseudospectral discretization

Let  $M \in \mathbb{N}$  be a fixed discretization index. We consider a mesh of nodes  $\Theta_M = \{\theta_0, \theta_1, \dots, \theta_M\} \subset \mathbb{R}_-$  such that

$$\theta_M < \dots < \theta_1 < \theta_0 = 0.$$

We will come back to the choice of the collocation nodes in Section 3.3.

Let  $\ell_j(\theta)$ ,  $j = 0, \dots, M$  be the Lagrange polynomials associated to  $\Theta_M$ ,

$$\ell_j(\theta) = \prod_{k \neq j} \frac{\theta - \theta_k}{\theta_j - \theta_k}, \quad j = 0, \dots, M.$$

Let  $\Pi_M^d$  be the space of  $\mathbb{R}^d$ -valued polynomials of degree less than or equal to  $M$  (notice that  $\Pi_M^d \cong \mathbb{R}^{(M+1)d}$ ).

Given  $\hat{\Phi}_0 \in \mathbb{R}^d$  and  $\hat{\Phi} = (\hat{\Phi}_1^T, \dots, \hat{\Phi}_M^T)^T \in \mathbb{R}^{Md}$  (where the superscript  $T$  denotes transposition, and we transpose twice in order to work with column vectors), we introduce the interpolation operator  $\hat{\mathcal{J}}_M: \mathbb{R}^d \times \mathbb{R}^{Md} \rightarrow w\Pi_M^d$  defined by

$$\hat{\mathcal{J}}_M(\hat{\Phi}_0, \hat{\Phi})(\theta) := w(\theta) \sum_{j=0}^M \ell_j(\theta) \frac{\hat{\Phi}_j}{w(\theta_j)}, \quad \theta \leq 0, \quad (14)$$

see [42]. A function  $\hat{\varphi}: \mathbb{R}_- \rightarrow \mathbb{R}^d$  is approximated by the interpolating function  $\hat{\varphi}_M := \hat{\mathcal{J}}_M(\hat{\Phi}_0, \hat{\Phi})$ , where  $\hat{\Phi}_j = \hat{\varphi}(\theta_j)$ ,  $j = 0, \dots, M$ . Notice that both  $\hat{\varphi}$  and  $\hat{\varphi}_M$  vanish at  $-\infty$ , and the interpolation scheme (14) is exact on functions  $\hat{\varphi} \in w\Pi_M^d$ . Moreover, when  $\hat{\varphi} = w\varphi$ , (14) is equivalent to approximating the function  $\varphi$  by the interpolating polynomial  $\mathcal{J}_M(\Phi_0, \Phi) \in \Pi_M^d$  defined by

$$\mathcal{J}_M(\Phi_0, \Phi)(\theta) := \sum_{j=0}^M \ell_j(\theta) \Phi_j, \quad \theta \leq 0,$$

where  $\Phi_j := \varphi(\theta_j)$  for  $j = 0, \dots, M$ , and  $\Phi = (\Phi_1^T, \dots, \Phi_M^T)^T$ . The reason for working with the operator  $\hat{\mathcal{J}}_M$  is mainly numerical, for avoiding instabilities in the computations [25, 38].

We now define the finite dimensional subspaces  $\hat{X}_M = w\Pi_M^{d_X} \subset X_M$  and  $\hat{Y}_M = w\Pi_M^{d_Y} \subset Y_M$ , and we project the ADE (13) into  $\hat{X}_M \times \hat{Y}_M$ . We approximate the pair  $(\hat{\varphi}, \hat{\psi}) \in D(\hat{\mathcal{A}})$  with  $(\hat{\varphi}_M, \hat{\psi}_M) \in \hat{X}_M \times \hat{Y}_M$ , and we approximate the action of  $\hat{\mathcal{A}}$  by collocation on the nodes  $\Theta_M$ : in particular, we impose the action (11) on  $\theta_1, \dots, \theta_M$  and we reserve the node  $\theta_0 = 0$  to impose the domain condition (12). The approximation of  $\hat{\mathcal{A}}$  is a finite dimensional operator represented by

$$\hat{A}_M: \mathbb{R}^{Md_X} \times \mathbb{R}^{d_Y} \times \mathbb{R}^{Md_Y} \rightarrow \mathbb{R}^{Md_X} \times \mathbb{R}^{d_Y} \times \mathbb{R}^{Md_Y}.$$

Given an element  $(\Phi, \mathbf{y}, \Psi) \in \mathbb{R}^{Md_X} \times \mathbb{R}^{d_Y} \times \mathbb{R}^{Md_Y}$ , the action of  $\hat{A}_M$  is

$$\hat{A}_M(\Phi, \mathbf{y}, \Psi) = (\Xi, \mathbf{z}, \Upsilon), \quad (15)$$

where

$$\begin{aligned}\Xi_j &= \hat{\mathcal{J}}_M(\mathbf{x}, \Phi)'(\theta_j) - \rho \Phi_j, \quad j = 1, \dots, M \\ \mathbf{z} &= \hat{G}(\hat{\mathcal{J}}_M(\mathbf{x}, \Phi), \hat{\mathcal{J}}_M(\mathbf{y}, \Psi)) \\ \Upsilon_j &= \hat{\mathcal{J}}_M(\mathbf{y}, \Psi)'(\theta_j) - \rho \Psi_j, \quad j = 1, \dots, M,\end{aligned}$$

and  $\mathbf{x}$  is implicitly defined by the nonlinear equation

$$\mathbf{x} = \hat{F}(\hat{\mathcal{J}}_M(\mathbf{x}, \Phi), \hat{\mathcal{J}}_M(\mathbf{y}, \Psi)). \quad (16)$$

As will become clear later on, the reason for handling separately the domain condition (16) is that we want to obtain an approximating system of ODEs. If  $F$  is linear in the first argument (like, for instance, in many models from population ecology), then (16) can be inverted explicitly by exploiting the linearity of  $\hat{\mathcal{J}}_M$ , so that we can write

$$\mathbf{x} = \hat{H}(\Phi, \mathbf{y}, \Psi)$$

with

$$\hat{H}(\Phi, \mathbf{y}, \Psi) = \left[ I_M - \hat{F}(w\ell_0, \hat{\mathcal{J}}_M(\mathbf{y}, \Psi)) \right]^{-1} \sum_{j=1}^M \frac{\Phi_j}{w(\theta_j)} \hat{F}(w\ell_j, \hat{\mathcal{J}}_M(\mathbf{y}, \Psi)).$$

Let us now introduce the variables  $\hat{U}(t) \in \mathbb{R}^{Md_x}$ ,  $V_0(t) \in \mathbb{R}^{d_y}$ ,  $\hat{V}(t) \in \mathbb{R}^{Md_y}$  for all  $t \geq 0$ . By means of the discrete operator  $\hat{A}_M$  we can write the system of ODEs

$$\frac{d}{dt}(\hat{U}(t), V_0(t), \hat{V}(t)) = \hat{A}_M(\hat{U}(t), V_0(t), \hat{V}(t)), \quad t > 0. \quad (17)$$

Equation (17) is a finite dimensional approximation of the ADE (5) and therefore in the following we will refer to it as the “discrete ADE.”

Given an initial condition

$$(\hat{U}(0), V_0(0), \hat{V}(0)) = (\hat{\Phi}, \psi(0), \hat{\Psi}),$$

we expect that, at any time  $t \geq 0$ , the functions  $\hat{\mathcal{J}}_M(U_0(t), \hat{U}(t))$  and  $\hat{\mathcal{J}}_M(V_0(t), \hat{V}(t))$  approximate  $\hat{u}(t)$  and  $\hat{v}(t)$ , respectively, where  $U_0(t) = \mathbf{x}$  is the solution of the implicit equation

$$\mathbf{x} = \hat{F}(\hat{\mathcal{J}}_M(\mathbf{x}, \hat{U}(t)), \hat{\mathcal{J}}_M(V_0(t), \hat{V}(t))). \quad (18)$$

Anyway, here we are not interested in the convergence of the solutions of the initial value problems, but we will focus on the dynamical properties of the system and the approximation of the long-time behavior.

By exploiting the representation (14) of the interpolation operator  $\hat{\mathcal{J}}_M$ , we can write explicitly the operator  $\hat{A}_M$  (15) and the discrete ADE (17). We define the matrix  $\hat{D}_M := (\hat{d}_{ij})_{i,j=1,\dots,M} \in \mathbb{R}^{M \times M}$  and the vector  $\hat{d}_M := (\hat{d}_{10}, \dots, \hat{d}_{M0})^T \in \mathbb{R}^M$  with elements

$$\hat{d}_{ij} := \left( \frac{w(\theta)}{w(\theta_j)} \ell_j(\theta) \right)' \Big|_{\theta_i}, \quad i = 1, \dots, M, \quad j = 0, \dots, M.$$

The differentiation matrix can be computed in an efficient and stable way, see for instance [41–43]. Now, exploiting the linearity of differentiation, we can write explicitly the operator (15) and substitute it into (17), to obtain the following representation of the discrete ADE (suppressing time-dependence for clarity)

$$\begin{cases} \frac{d}{dt}\hat{U} = \hat{d}_M \otimes U_0 + (\hat{D}_M \otimes I_{d_X})\hat{U} - \rho\hat{U} \\ \frac{d}{dt}V_0 = \hat{G}\left(\hat{\mathcal{J}}_M(U_0, \hat{U}), \hat{\mathcal{J}}_M(V_0, \hat{V})\right) \\ \frac{d}{dt}\hat{V} = \hat{d}_M \otimes V_0 + (\hat{D}_M \otimes I_{d_Y})\hat{V} - \rho\hat{V}, \end{cases} \quad (19)$$

where  $\otimes$  denotes the tensor product and, at any time  $t \geq 0$ ,  $U_0(t) = \mathbf{x}$  is the solution of (18). System (19) has dimension  $\bar{d} := Md_X + (M+1)d_Y$ . We stress also that when  $F$  and  $G$  are bilinear maps, (19) is linear and the operator  $\hat{A}_M$  is represented by a matrix in  $\mathbb{R}^{\bar{d} \times \bar{d}}$ .

It is important to notice that the matrix  $\hat{D}_M$  and the vector  $\hat{d}_M$  are completely defined by the nodes  $\Theta_M$  and do not depend on the specific right-hand sides  $\hat{F}$  and  $\hat{G}$  of the delay equations under study. This makes it possible to write a code that automatically constructs the main part of the discrete ADE (19) from the nodes once the discretization index  $M$  is given, while the user only needs to specify the equations involving  $\hat{F}$  and  $\hat{G}$ .

Since we aim at approximating the long-term behavior and the bifurcation properties of systems of type (1), it is important to verify that the discrete ADE (19) preserves the dynamical properties of the original equation at least for  $M$  large enough. In the case of equilibria the correspondence is one-to-one, as proved in the following theorem.

**Theorem 4** (Correspondence of equilibria). *If the constant mapping  $(\bar{x}, \bar{y}) \in X \times Y$  is an equilibrium of (1), then  $(\bar{U}, \bar{y}, \bar{V}) \in \mathbb{R}^{\bar{d}}$  with*

$$\begin{aligned} \bar{U}_j &= \bar{x}w(\theta_j) \\ \bar{V}_j &= \bar{y}w(\theta_j), \end{aligned} \quad j = 1, \dots, M, \quad (20)$$

*is an equilibrium of (19). Vice versa, if  $(\bar{U}, \bar{y}, \bar{V})$  is an equilibrium of (19) and  $\bar{x}$  is the solution of*

$$\bar{x} = \hat{F}(\hat{\mathcal{J}}_M(\bar{x}, \bar{U}), \hat{\mathcal{J}}_M(\bar{y}, \bar{V})), \quad (21)$$

*then (20) holds and  $(\bar{x}, \bar{y})$  is an equilibrium of (1).*

**PROOF.** Assume  $(\bar{x}, \bar{y})$  is an equilibrium of (1) and define  $(\bar{U}, \bar{y}, \bar{V})$  as in (20). Then,  $\hat{\mathcal{J}}_M(\bar{x}, \bar{U}) = \bar{x}w$  and  $\hat{\mathcal{J}}_M(\bar{y}, \bar{V}) = \bar{y}w$ . Moreover

$$\hat{d}_M \otimes \bar{x} + (\hat{D}_M \otimes I_{d_X})\bar{U} - \rho\bar{U} = \hat{\mathcal{J}}_M(\bar{x}, \bar{U})'(\Theta_M) - \rho\bar{U} = \bar{x}w'(\Theta_M) - \rho\bar{U} = 0,$$

and analogously

$$\hat{d}_M \otimes \bar{y} + (\hat{D}_M \otimes I_{d_Y})\bar{V} - \rho\bar{V} = 0.$$

Hence  $(\bar{U}, \bar{y}, \bar{V})$  is an equilibrium of (19).

Assume now  $(\bar{U}, \bar{y}, \bar{V})$  is an equilibrium of (19) and let  $\bar{x}$  be defined by (21). Since  $\hat{\mathcal{J}}_M(\bar{x}, \bar{U})/w$  is a polynomial of degree at most  $M$  and its derivative vanishes in  $\theta_j$ ,  $j = 1, \dots, M$ , it follows that it is in fact constant, and hence  $\hat{\mathcal{J}}_M(\bar{x}, \bar{U}) = \bar{x}w$ . Analogously,  $\hat{\mathcal{J}}_M(\bar{y}, \bar{V}) = \bar{y}w$ , from which (20) follows. Finally, the equilibrium conditions (7) hold.

Thanks to Theorem 2, in order to prove that the discretization not only preserves equilibria but also their local stability properties, we should compare the linearized systems and verify that the eigenvalues of the linear infinitesimal generator  $\hat{\mathcal{A}}$  that lie in  $\mathbb{C}_\rho$  are well approximated by the eigenvalues of  $\hat{A}_M$  for  $M$  large enough. It is easy to show that the pseudospectral discretization commutes with linearization at an equilibrium. Hence, the problem reduces to proving that, for linear equations, the spectrum of the discretized infinitesimal generator  $\hat{A}_M$  approximates the eigenvalues of  $\hat{\mathcal{A}}$  in  $\mathbb{C}_\rho$  as  $M \rightarrow \infty$ , and that no spurious eigenvalues are introduced in  $\mathbb{C}_\rho$  by the discretization. We leave for a future work the rigorous proof of convergence, which follows the lines of [8], while in Section 4 we support this conjecture with some numerical tests.

### 3.3. The collocation nodes

The numerical procedure presented above can be applied for any choice of the nodes  $\Theta_M$ . However, the collocation nodes are of great importance for the accuracy of the approximation [37]. In our case, one possible choice is to look at the Gaussian nodes associated to the Laguerre polynomials, which are orthonormal with respect to the exponential weight [38]. Since the node  $\theta_0 = 0$  should belong to  $\Theta_M$  in order to include the boundary condition defining the domain of the infinitesimal generator (cf. (4) or (12)), we consider the nodes of Radau type, i.e., the abscissa corresponding to the extrema of the Laguerre polynomials and the additional node  $\theta_0 = 0$ .

We also recall that, because the unbounded interval can be mapped onto itself via multiplication with any positive factor, a finite set of nodes involves two different degrees of freedom: the size of the mesh (determined by the index  $M$ ) and a positive scaling parameter (that will be linked to  $\rho$ ), see, e.g., [2, 42]. We first introduce the standard Laguerre–Gauss–Radau (LGR) nodes in  $\mathbb{R}_+$  and then we will show how to suitably scale the nodes in order to capture the asymptotic behavior of the functions of interest, which belong to the space  $X_\rho \times Y_\rho$ .

Let  $\mathcal{L}_n(s)$ ,  $n \in \mathbb{N}$ ,  $s \in \mathbb{R}_+$ , be the family of standard Laguerre polynomials of degree  $n$ , orthonormal with respect to the weight  $e^{-s}$ , i.e.,

$$\int_0^{+\infty} e^{-s} \mathcal{L}_m(s) \mathcal{L}_n(s) ds = \delta_{mn}, \quad m, n \in \mathbb{N}.$$

For further details about the properties of these polynomials and for the theory introduced in this section, see [27, 38, 39] and references therein.

Given a discretization index  $M \in \mathbb{N}$ , the classical LGR nodes  $\{s_0, \dots, s_M\} \subset \mathbb{R}_+$  are defined as the zeros of  $s\mathcal{L}'_{M+1}(s)$ , i.e.,  $s_1, \dots, s_M$  are the abscissa corresponding to the extrema of  $\mathcal{L}_{M+1}(s)$  to which we add the node  $s_0 = 0$ . Let  $\omega_j$ ,  $j = 0, \dots, M$ , be the weights of the Gauss–Radau quadrature formula

$$\int_0^{+\infty} e^{-s} \varphi(s) ds \approx \sum_{j=0}^M \varphi(s_j) \omega_j,$$

that evaluates exactly the weighted integral when  $\varphi \in \Pi_{2M}$ . MATLAB codes for the computation of the LGR nodes and the corresponding weights are available for instance at [26, 41], see also [27, 38].

We move now to the negative half line  $\mathbb{R}_-$ . We consider a positive scaling parameter  $\rho > 0$  and we define the scaled Laguerre functions  $\hat{\mathcal{L}}_n(\theta) = e^{\rho\theta} \mathcal{L}_n(-2\rho\theta)$ ,  $n \in \mathbb{N}$ ,  $\theta \leq 0$ , such that

$$\int_{-\infty}^0 \hat{\mathcal{L}}_m(\theta) \hat{\mathcal{L}}_n(\theta) d\theta = \delta_{mn}, \quad m, n \in \mathbb{N}.$$

Since  $\lim_{\theta \rightarrow -\infty} \hat{\mathcal{L}}_n(\theta) = 0$ , working with Laguerre functions instead of Laguerre polynomials allows to avoid unstable operations and round-off errors when computing the corresponding nodes, quadrature weights and differentiation matrices as well as interpolating functions, as remarked for instance in [2, 25, 38, 39]. On  $\mathbb{R}_-$ , we define the scaled nodes

$$\theta_j := -\frac{s_j}{2\rho}, \quad j = 0, \dots, M.$$

The corresponding Gauss–Radau quadrature formula is

$$\int_{-\infty}^0 e^{\rho\theta} \hat{\varphi}(\theta) d\theta = \sum_{j=0}^M \hat{\varphi}(\theta_j) \hat{\omega}_j, \quad (22)$$

where

$$\hat{\omega}_j := \frac{\omega_j}{2\rho} e^{-\rho\theta_j}, \quad j = 0, \dots, M,$$

and it is exact on  $\hat{\varphi} = w\varphi$ , with  $\varphi \in \Pi_{2M}$ . The weights  $\hat{\omega}_j$  can be computed with stable algorithms [26, 27].

In the numerical simulations of the next section, we will exploit the freedom in the choice of the state space  $X_\rho \times Y_\rho$  (cf. Theorem 1) to tune appropriately the scaling parameter  $\rho$  in order to take advantage of the exactness of the quadrature formula (22). Notice that in any case we should take  $2\rho \leq \bar{\rho}$ , where  $\bar{\rho}$  characterizes the maximal space on which  $F$  and  $G$  are defined.

#### 4. Numerical tests

In this section we want to validate numerically the technique and show how it can be effectively exploited to study the bifurcation properties of nonlinear models of the form (1) by applying available software for ODEs like the toolbox MATCONT [17, 28], to the discrete ADE (19) obtained through pseudospectral discretization. We choose MATCONT because it is compatible with the widespread software MATLAB, but we stress that the discrete ADE can be analyzed with any bifurcation package for ODEs. Among its many features, MATCONT performs the numerical continuation of equilibria and periodic solutions with respect to one or two parameters, the computation of stability of the attractors, and the automatic detection of singularities and bifurcation points on the curves by computing suitable test functions. Moreover, it is possible to control the accuracy in the output by means of MATCONT continuation options, that allow to impose the desired tolerance on the nonlinear solvers and on the test functions. We will exploit these possibilities for the bifurcation analysis of some nonlinear equations with infinite delay. We will test the outcome quantitatively by exploiting the MATCONT tolerance options to ensure a certain high accuracy in the output, and we will compare the results

with some reference values obtained through an alternative equivalent formulation of the models.

However, before dealing with nonlinear equations, it is important to remember that the stability of an equilibrium is determined by the part of the spectrum of the infinitesimal generator of the linearization (8) which lies in  $\mathbb{C}_\rho$ , and, as described in Section 2, contains only eigenvalues. Hence, we will first consider linear equations and investigate how accurately the eigenvalues of the associated linear operator  $\hat{\mathcal{A}}$  are approximated by the spectrum of the discrete operator  $\hat{A}_M$  when increasing the discretization index  $M$ .

#### 4.1. Linear equations: approximation of eigenvalues

First of all we consider the trivial delay differential equation corresponding to  $d_X = 0$ ,  $d_Y = 1$ , and  $G = 0$ ,

$$\frac{dy}{dt}(t) = 0, \quad t > 0. \quad (23)$$

The state  $y_t$  belongs to  $Y_\rho$  for any  $\rho > 0$ . Let  $\mathcal{A}_0: D(\mathcal{A}_0)(\subseteq Y_\rho) \rightarrow Y_\rho$  be the infinitesimal generator of the family of solution operators  $\{T_0(t)\}_{t \geq 0}$ , where

$$T_0(t)(\psi)(\theta) = \begin{cases} \psi(t + \theta) & \theta \in (-\infty, -t] \\ \psi(0) & \theta \in (-t, 0]. \end{cases}$$

The spectrum of  $\mathcal{A}_0$  contains only the (simple) eigenvalue  $\lambda = 0$  corresponding to the constant eigenfunction  $\psi(\theta) = c$ , for  $c \in \mathbb{C} \setminus \{0\}$ .

Fix now an arbitrary  $\rho > 0$  and let  $\hat{A}_{0,M}$  be the pseudospectral discretization of  $\hat{\mathcal{A}}_0$  on the nodes  $\Theta_M$ . In matrix notation,

$$\hat{A}_{0,M} = \begin{pmatrix} 0 & 0 & \cdots & 0 \\ \hat{d}_M & \hat{D}_M - \rho I_M & & \end{pmatrix} \in \mathbb{R}^{(M+1) \times (M+1)}.$$

The matrix  $\hat{A}_{0,M}$  has  $M + 1$  eigenvalues counted with their multiplicity and, as  $M \rightarrow \infty$ , one of them should approximate the unique eigenvalue of  $\hat{\mathcal{A}}_0$ ,  $\lambda = 0$ . We want to investigate how the other  $M$  eigenvalues are located with respect to  $\mathbb{C}_\rho$ , depending on the choice of the collocation nodes. This is the main reason for including the trivial equation (23) in our numerical tests.

In Figure 1(a) we plotted the computed spectrum of  $\hat{A}_{0,M}$  for different values of  $M$ , with  $\rho = 0.5$  and  $\rho = 1$ , when the collocation nodes are the LGR nodes defined in Section 3.3. The eigenvalue  $\lambda = 0$  is accurate to the machine precision *eps*, while the other  $M$  eigenvalues are aligned along the vertical line  $\Re(\lambda) = -\rho$  of the complex plane. We will refer to the latter as “uninteresting” eigenvalues, since they do not contribute to the approximation of the spectrum of the infinitesimal generator in  $\mathbb{C}_\rho$ . The special configuration of the eigenvalues of  $\hat{A}_{0,M}$  for a given  $\rho > 0$  suggests that the pseudospectral discretization technique on LGR nodes is a good approach for the problem at hand.

The distribution of the uninteresting eigenvalues is strictly linked to the choice of the collocation nodes, as we can see by comparing the upper and lower panels of Figure 1. Figure 1(b) represents the eigenvalues of  $\hat{A}_{0,M}$  for the same parameters  $M$  and  $\rho$ , but where the nodes are the Laguerre–Gauss points (see, e.g., [38]), viz., the roots of  $s\mathcal{L}_M(s)$  divided by the scaling constant  $-2\rho$  as explained in Section 3.3. We observe that for

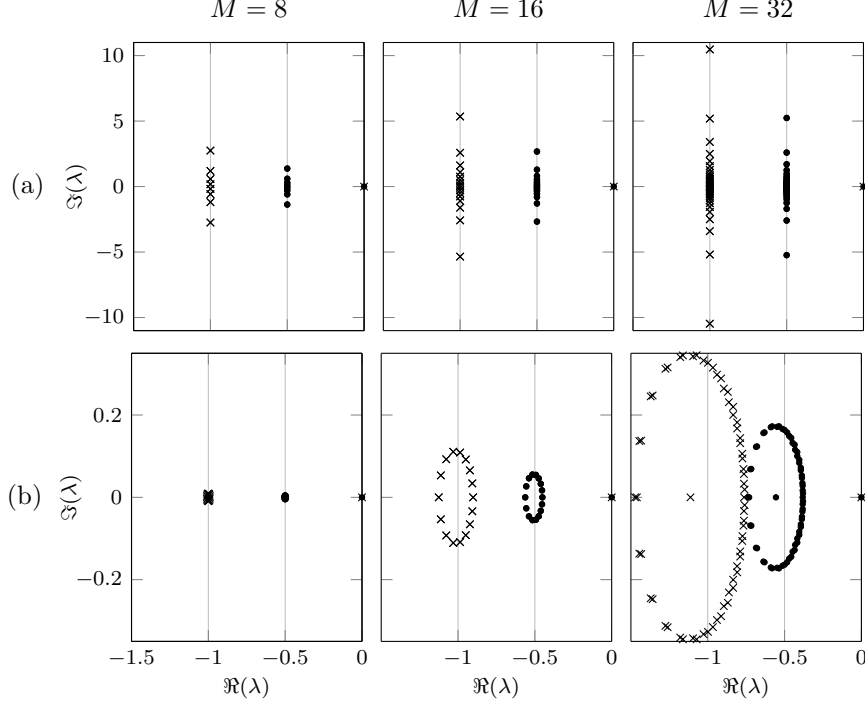


Figure 1: computed eigenvalues of  $\hat{A}_{0,M}$  for  $\rho = 0.5$  (dots) and  $\rho = 1$  (crosses), for different values of  $M$  and (a) Laguerre–Gauss–Radau and (b) Laguerre–Gauss collocation nodes.

both choices of the nodes the eigenvalue  $\lambda = 0$  is approximated to the machine precision *eps* and the other eigenvalues remain in the negative half of the complex plane, but in the second case they expand into  $\mathbb{C}_\rho$  as  $M$  increases, thus possibly interfering with the approximation of the true eigenvalues in  $\mathbb{C}_\rho$ . Such numerical evidence further motivates our preference for LGR points as collocation nodes for the infinite delay.

We now consider a nontrivial linear equation for which the characteristic roots (which, as explained in Section 2, coincides in  $\mathbb{C}_\rho$  with the eigenvalues of the linear infinitesimal generator  $\hat{\mathcal{A}}$ ) are explicitly available, and we investigate numerically the convergence of the eigenvalues of the discrete operator  $\hat{A}_M$  to those of  $\hat{\mathcal{A}}$  when increasing the discretization index  $M$ .

Consider the scalar linear delay differential equation

$$\frac{dy}{dt}(t) = ay(t) + \int_0^{+\infty} b(s)y(t-s) ds, \quad t > 0,$$

for  $a \in \mathbb{R}$  and  $b \in L^1(\mathbb{R}_-, \mathbb{R})$ . The corresponding characteristic equation is

$$\lambda = a + \mathcal{L}(b)(\lambda),$$

where  $\mathcal{L}(b)$  is the Laplace transform of  $b$ . We now take an exponential kernel of the form

$$b(s) = b_0 e^{-\mu s} \tag{24}$$

for  $b_0 \in \mathbb{R}$  and  $\mu > 0$ , so that the Laplace transform is explicitly available:

$$\mathcal{L}(b)(\lambda) = \frac{b_0}{\lambda + \mu}, \quad \text{for } \Re(\lambda) > -\mu.$$

By writing  $\lambda = \alpha + i\beta$  for  $\alpha, \beta \in \mathbb{R}$ ,  $\beta \geq 0$ , we can solve the characteristic equation explicitly and get

$$\alpha = \frac{a - \mu}{2}, \quad \beta^2 = -b_0 - \left(\frac{a + \mu}{2}\right)^2. \quad (25)$$

Notice that a necessary condition for the existence of characteristic roots is

$$b_0 \leq -\left(\frac{a + \mu}{2}\right)^2.$$

The freedom in the choice of  $\rho$  (cf. Section 2) and the kernel (24) motivate to choose  $\rho = \mu/2$ , so that the quadrature formula (22) on the corresponding LGR nodes  $\Theta_M$  is exact on functions  $\hat{\varphi} = w\varphi$ , with  $\varphi \in \Pi_{2M}$ . The discretization  $\hat{A}_M$  of  $\hat{A}$  is

$$\hat{A}_M = \begin{pmatrix} a + B_0 & B_1 & \cdots & B_M \\ \hat{d}_M & \hat{D}_M - \rho I_M & & \end{pmatrix} \in \mathbb{R}^{(M+1) \times (M+1)}, \quad (26)$$

where

$$B_j := e^{-\rho\theta_j} \int_0^{+\infty} b(s)\ell_j(-s) ds = b_0\hat{\omega}_j, \quad j = 0, \dots, M.$$

In what follows we test the convergence of the eigenvalues of  $\hat{A}_M$  (26) to the exact characteristic roots  $\lambda = \alpha + i\beta$  (25) when increasing the discretization index  $M$ . We choose different values of the parameters  $a$ ,  $b_0$ ,  $\mu$ , in order to investigate how the convergence with respect to  $M$  is influenced by the multiplicity of  $\lambda$ , by the modulus and the real part of  $\lambda$ , and by the choice of  $\rho$ . In all the cases we take  $\alpha > -\rho$ .

The results are plotted in Figures 2-3: the left panels show the exact characteristic roots  $\lambda$  and the computed eigenvalues of  $\hat{A}_M$ , while the right panels show the absolute error in the approximation of  $\lambda$  when increasing  $M$ . In all the simulations, the uninteresting eigenvalues are slightly perturbed from the vertical line  $\Re(\lambda) = -\rho$ . Our simulations showed that the characteristic roots located to the left of the uninteresting eigenvalues are not approximated by the discretization. Anyway, such roots are not relevant for stability and we did not include those tests here. When the characteristic roots are located to the right of the uninteresting eigenvalues, all the error plots exhibit the typical trend of spectral convergence, i.e., the error decays faster than  $O(M^{-k})$  for any  $k > 0$ . The numerical simulations highlight three different aspects influencing the accuracy guaranteed by a certain discretization index  $M$ .

- (i) The accuracy in the approximation of  $\lambda$  depends on the multiplicity of  $\lambda$  as a root of the characteristic equation, as proved in [8] in the case of finite delay. Indeed, the complex conjugate pairs can be approximated to the machine precision *eps* by taking  $M$  large enough, see Figure 2(b) and (c), whereas the convergence to the double real eigenvalue stops at  $\sqrt{\epsilon ps}$ , see Figure 2(a).
- (ii) Fixed  $M$ , a smaller  $|\lambda|$  allows for better accuracy in the approximation, as emerging from the comparison of Figure 3(a) and (b), where the complex conjugate pair of eigenvalues have the same zero real part, but different modulus.



- (iii) Fixed  $M$ , a larger  $\rho$  allows for better accuracy, as emerging by comparing Figure 3(b) and (c), where we consider the same couple of imaginary eigenvalues, but different values of  $\rho$ .

As a final remark, by comparing the simulations in this study with those performed in [4, 5, 8] in the case of finite delay, we observe that the discretization of equations with infinite delay requires in general higher values of  $M$  to reach the same accuracy.

#### 4.2. A nonlinear delay differential equation

Now we turn our attention to nonlinear equations. We want to show with some numerical examples how the pseudospectral discretization technique provides an effective and flexible tool for studying numerically the bifurcation properties of delay equations by using software for ODEs like, for instance, the continuation package MATCONT for MATLAB.

Consider the nonlinear delay differential equation

$$\frac{dy}{dt}(t) = -\delta_A y(t) + b \int_0^{+\infty} f_{n/\tau}^{(n)}(s) e^{-\delta_J s - a y(t-s)} y(t-s) ds, \quad (27)$$

where  $\tau, n, a, b, \delta_A, \delta_J$  are positive parameters and, given  $\alpha > 0$  and  $n > 0$ ,  $f_\alpha^{(n)}(s)$  is the Gamma distribution

$$f_\alpha^{(n)}(s) = \frac{\alpha^n s^{n-1} e^{-\alpha s}}{\Gamma(n)}, \quad s \geq 0.$$

Equation (27) is studied in [1] as an equation describing the evolution of a single-species adult population where the maturation age of an individual is continuously distributed over time according to the Gamma distribution. The authors prove that, if  $n$  is large enough, the nontrivial equilibrium undergoes two Hopf bifurcations when varying the parameter  $\tau$  representing the expected maturation age. For smaller values of  $n$  no stability switch occurs, the nontrivial equilibrium being locally asymptotically stable whenever it exists positive.

If  $n \in \mathbb{N}$ , by introducing the auxiliary variables

$$z_j(t) := \int_0^{+\infty} \frac{\alpha^n}{(n-1)!} e^{-(\alpha+\delta_J)s} s^j e^{-a y(t-s)} y(t-s) ds, \quad j = 0, \dots, n-1,$$

and using the technique explained in [19, 31, 36] we can formulate equation (27) equivalently as the  $(n+1)$ -dimensional system of ODEs

$$\begin{cases} \frac{dz_0}{dt} = -(\alpha + \delta_J)z_0 + \frac{\alpha^n}{(n-1)!} e^{-a y} y \\ \frac{dz_1}{dt} = z_0 - (\alpha + \delta_J)z_1 \\ \vdots \\ \frac{dz_{n-1}}{dt} = (n-1)z_{n-2} - (\alpha + \delta_J)z_{n-1} \\ \frac{dy}{dt} = bz_{n-1} - \delta_A y. \end{cases} \quad (28)$$

The reformulation in terms of ODEs allows the comparison of the bifurcation analysis performed with MATCONT on the pseudospectral discretization of (27) and on the system of ODEs (28).

We first applied MATCONT to obtain the numerical bifurcation diagram with respect to the parameter  $\tau$ . In Figure 4 we compared the diagram computed from system (28) with the one computed from the pseudospectral discretization of (27) with  $M = 10$  and  $\rho = (\delta_J + n/\tau)/4$ , with MATCONT tolerance TOL=  $10^{-10}$  and model parameters specified in the caption. The parameter  $M$  is chosen to balance high accuracy and low computational time. The parameter  $\rho$  is tuned in order to improve the accuracy of the quadrature formula (22). In accordance with the theoretical analysis in [1], for  $n = 5$  no bifurcation is detected on the nontrivial equilibrium branch, see Figure 4, left panel. For  $n = 7$  (right panel), two Hopf bifurcation points  $H_1$  and  $H_2$  are detected at  $\tau_1 \approx 1.55$  and  $\tau_2 \approx 3.13$ . MATCONT allows to continue the branch of periodic solutions arising from a Hopf bifurcation point: the maximum and minimum value of the branch of periodic orbits are also included in the figure. We stress the remarkable overlapping between the bifurcation diagram of the pseudospectral discretization and the reference diagram obtained from (28).

Differently from (28), the pseudospectral discretization of (27) allows to perform the numerical continuation of the Hopf bifurcation curve in the two-parameter plane  $(\tau, n)$  with  $n \in \mathbb{R}_+$ . The computed curve is plotted in Figure 5, and clearly shows that the stability switch through Hopf bifurcation is lost for small values of  $n$ , as proved in [1].

We finally studied the convergence of the Hopf bifurcation points detected during the MATCONT continuation for  $n = 7$  shown in Figure 4, right panel. Figure 7 (left) shows the absolute error between the Hopf values computed from the pseudospectral discretization of (27) and the reference values  $\tau_1$  and  $\tau_2$  computed from the system of ODEs (28), when increasing the index  $M$ . All the simulations are performed with MATCONT tolerance TOL=  $10^{-10}$ . The plot provides numerical evidence of the convergence of the bifurcation points as  $M$  increases, and the error exhibits the typical spectral decaying behavior.

#### 4.3. A physiologically structured population model

Consider the following model for a physiologically structured population, introduced in [16] as a simplified version of the model for *Daphnia* presented in [34],

$$\begin{cases} b(t) = \frac{\alpha S(t)}{1 + S(t)} \int_0^{+\infty} e^{-\mu s} b(t-s) \ell(s; S_t)^2 ds \\ \frac{dS}{dt}(t) = rS(t) \left(1 - \frac{S(t)}{K}\right) - \frac{S(t)}{1 + S(t)} \int_0^{+\infty} e^{-\mu s} b(t-s) \ell(s; S_t)^2 ds, \end{cases} \quad (29)$$

where  $\alpha, \mu, r, K$  are positive parameters and  $\ell(s; S_t)$  is the length of an individual that has age  $s$  at time  $t$ , defined by

$$\ell(s; S_t) := \int_0^s \frac{S(t-a)}{1 + S(t-a)} e^{-a} da.$$

By introducing the auxiliary variables

$$z_j(t) := \int_0^{+\infty} b(t-s) e^{-\mu s} \ell(s; S_t)^j ds, \quad j = 0, 1, 2,$$

we can write the equivalent system of ODEs

$$\begin{cases} \frac{dz_0}{dt} = -\mu z_0 + \frac{\alpha S z_2}{1+S} \\ \frac{dz_1}{dt} = \frac{S z_0}{1+S} - (\mu + 1) z_1 \\ \frac{dz_2}{dt} = \frac{2S z_1}{1+S} - (\mu + 2) z_2 \\ \frac{dS}{dt} = rS \left(1 - \frac{S}{K}\right) - \frac{S z_2}{1+S}, \end{cases} \quad (30)$$

and  $b(t) = \frac{\alpha S z_2}{1+S}$ . Therefore we can again compare numerically the bifurcation analysis performed with MATCONT on system (30) and on the pseudospectral discretization of (29).

In Figure 6 we plotted the numerical bifurcation diagram of  $S$  with respect to the parameter  $K$  (left panel) and the existence and stability regions of the nontrivial equilibrium in the plane  $(K, \alpha)$  (right panel). The model parameters are specified in the caption. In the figure, the bifurcation diagram of the pseudospectral discretization of (29) for  $M = 20$  and  $\rho = \mu/2$  is superimposed to the one of the reference system of ODEs (30), showing a remarkable fit.

Figure 7 (right) shows the error in the detection of the transcritical bifurcation (branching point of the equilibrium curve)  $K_{BP} \approx 2.02$ , and the Hopf bifurcation  $K_H \approx 5.88$ , obtained from the pseudospectral discretization of (29) with parameter values specified in the caption of Figure 6, compared to the reference values obtained from system (30). The transcritical bifurcation point is approximated to the tolerance  $10^{-8}$  already for  $M = 1$ , while the error in the Hopf shows spectral convergence when increasing  $M$ .

## 5. Conclusions and open problems

This study takes a step forward towards the goal of a numerical toolbox for the automatic bifurcation analysis of nonlinear delay equations, including integral and integro-differential equations. The pseudospectral discretization of equations with finite delay proposed in [4] has been here extended to the case of unbounded delay, thus showing once more the wide applicability of the approach. When applied to nonlinear delay equations, the pseudospectral discretization technique provides an approximating system of ODEs with several advantages:

- the technique applies to discrete and distributed delays, renewal and delay differential equations, finite and infinite delays (with a suitable choice of the collocation nodes), thus ensuring a fair generality;
- the numerical evidence indicates a spectral convergence of the approximations when increasing the discretization index  $M$ , so an index of order of tens is usually enough to reach a satisfactory accuracy for applications;
- the bifurcation properties of the system can be numerically investigated with well-established software for ODEs without requiring *ad hoc* software, thus allowing to understand some properties that are otherwise impossible to study analytically;
- from the point of view of a user (who is familiar with bifurcation software for ODEs), the major part of the system can be built automatically when the discretization

index  $M$  is given: hence, this part of the algorithm can be implemented once for all, and when studying a different model the user should only adapt the code by substituting the specific right-hand side;

- the technique does not require a specific treatment or modification of the right-hand sides of the delay equation, since they appear in the approximating system simply as applied to interpolating polynomials.

All these reasons together suggest that the pseudospectral discretization approach is suitable for providing to a wide public of users a numerical tool for studying mathematical models involving delays. Anyway, since the dimension of the discrete ADE (19) is usually considerably larger than the dimension of the original delay equation, computational time may be significant. Especially complex applications like realistic models of physiologically structured populations, which involve for example external ODEs for the individual growth and time- or state-dependent maturation delays, may prove to be challenging from a computational perspective, requiring a special treatment and optimization of the codes. We are interested in carrying this analysis further on by testing the technique on some realistic models.

The investigation contained in this paper is mainly numerical, aiming at providing concrete evidence of the effectiveness and flexibility of the approach. The rigorous proof that the discrete ADE reproduces the stability properties of the equilibria of the delay equation is ongoing. The proof requires the theoretical analysis of the convergence of the characteristic roots in the linear case and follows the ideas presented in [8].

## 6. Acknowledgments

The authors thank Odo Diekmann for valuable comments on an earlier draft of the manuscript.

## 7. Funding

The work of M.G. and F.S. was partially supported by the Centre of Excellence in Analysis and Dynamics Research (Academy of Finland). The work of R.V. was supported by INdAM GNCS 2017 project “Analisi e sviluppo di metodologie numeriche per certi tipi non classici di sistemi dinamici.”

## 8. Bibliography

- [1] BERETTA, E., AND BREDÁ, D. Discrete or distributed delay? Effects on stability of population growth. *Math. Biosci. Eng.* 13, 1 (2016), 19–41.
- [2] BOYD, J. P. *Chebyshev and Fourier spectral methods*, second ed. Dover Publications, Inc., Mineola, NY, 2001.
- [3] BREDÁ, D., DIEKMANN, O., DE GRAAF, W. F., PUGLIESE, A., AND VERMIGLIO, R. On the formulation of epidemic models (an appraisal of Kermack and McKendrick). *J. Biol. Dyn.* 6, 2 (2012), 103–117.
- [4] BREDÁ, D., DIEKMANN, O., GYLLENBERG, M., SCARABEL, F., AND VERMIGLIO, R. Pseudospectral discretization of nonlinear delay equations: new prospects for numerical bifurcation analysis. *SIAM J. Appl. Dyn. Syst.* 15, 1 (2016), 1–23.

- [5] BREDA, D., DIEKMANN, O., LIESSI, D., AND SCARABEL, F. Numerical bifurcation analysis of a class of nonlinear renewal equations. *Electron. J. Qual. Theory Differ. Equ.* 64 (2016), 1–24.
- [6] BREDA, D., GETTO, P., SÁNCHEZ SANZ, J., AND VERMIGLIO, R. Computing the eigenvalues of realistic Daphnia models by pseudospectral methods. *SIAM J. Sci. Comput.* 37, 6 (2015), 2607–2629.
- [7] BREDA, D., MASET, S., AND VERMIGLIO, R. TRACE-DDE. <https://users.dimi.uniud.it/~dimitri.breda/research/software/>. Accessed: 03.04.2017.
- [8] BREDA, D., MASET, S., AND VERMIGLIO, R. Pseudospectral differencing methods for characteristic roots of delay differential equations. *SIAM J. Sci. Comput.* 27, 2 (2005), 482–495.
- [9] BREDA, D., MASET, S., AND VERMIGLIO, R. *Stability of linear delay differential equations. A numerical approach with MATLAB*. SpringerBriefs in Electrical and Computer Engineering, Springer, New York, 2015.
- [10] CLÉMENT, P., DIEKMANN, O., GYLLENBERG, M., HEIJMANS, H. J. A. M., AND THIEME, H. R. Perturbation theory for dual semigroups. I. The sun-reflexive case. *Math. Ann.* 277, 4 (1987), 709–725.
- [11] CLÉMENT, P., DIEKMANN, O., GYLLENBERG, M., HEIJMANS, H. J. A. M., AND THIEME, H. R. Perturbation theory for dual semigroups. II. Time-dependent perturbations in the sun-reflexive case. *Proc. Roy. Soc. Edinburgh Sect. A* 109, 1-2 (1988), 145–172.
- [12] CLÉMENT, P., DIEKMANN, O., GYLLENBERG, M., HEIJMANS, H. J. A. M., AND THIEME, H. R. Perturbation theory for dual semigroups. III. Nonlinear Lipschitz continuous perturbations in the sun-reflexive case. In *Volterra integrodifferential equations in Banach spaces and applications (Trento, 1987)*, vol. 190 of *Pitman Res. Notes Math. Ser.* Longman Sci. Tech., Harlow, 1989, pp. 67–89.
- [13] CRANDALL, M. G., AND LIGGETT, T. M. Generation of semi-groups of nonlinear transformations on general Banach spaces. *Amer. J. Math.* 93 (1971), 265–298.
- [14] CRANDALL, M. G., AND PAZY, A. Semi-groups of nonlinear contractions and dissipative sets. *J. Functional Analysis* 3 (1969), 376–418.
- [15] DE ROOS, A. M. PSPM analysis. <https://bitbucket.org/amderoos/pspmanalysis>. Accessed: 03.04.2017.
- [16] DE ROOS, A. M. *Daphnids on a train: Development and application of a new numerical method for physiologically structured population models*. PhD thesis. Leiden University, 1989.
- [17] DHOOGHE, A., GOVAERTS, W., AND KUZNETSOV, Y. A. MATCONT: a MATLAB package for numerical bifurcation analysis of ODEs. *ACM Trans. Math. Software* 29, 2 (2003), 141–164.
- [18] DIEKMANN, O., AND GYLLENBERG, M. Equations with infinite delay: blending the abstract and the concrete. *J. Differential Equations* 252, 2 (2012), 819–851.
- [19] DIEKMANN, O., GYLLENBERG, M., AND METZ, J. A. J. Finite dimensional state representation of linear and nonlinear delay systems. Submitted.
- [20] DIEKMANN, O., GYLLENBERG, M., METZ, J. A. J., NAKAOKA, S., AND DE ROOS, A. M. *Daphnia revisited: local stability and bifurcation theory for physiologically structured population models explained by way of an example*. *J. Math. Biol.* 61, 2 (2010), 277–318.
- [21] DIEKMANN, O., VAN GILS, S. A., VERDUYN LUNEL, S. M., AND WALTHER, H.-O. *Delay equations. Functional, complex, and nonlinear analysis*, vol. 110 of *Applied Mathematical Sciences*. Springer-Verlag, New York, 1995.
- [22] DOEDEL, E. AUTO. Software for continuation and bifurcation problems in ordinary differential equations. <http://indy.cs.concordia.ca/auto/>. Accessed: 03.04.2017.
- [23] ENGELBORGH, K., LUZYANINA, T., SAMAËY, G., ROOSE, D., AND VERHEYDEN, K. DDE-BIFTOOL: a MATLAB package for bifurcation analysis of delay differential equations. <http://twr.cs.kuleuven.be/research/software/delay/ddebiftool.shtml>. Accessed: 03.04.2017.
- [24] ERMENROUT, B. XPP. <http://www.math.pitt.edu/~bard/xpp/xpp.html>. Accessed: 03.04.2017.
- [25] FUNARO, D. *Polynomial approximation of differential equations*, vol. 8 of *Lecture Notes in Physics. New Series m: Monographs*. Springer-Verlag, Berlin, 1992.
- [26] GAUTSCHI, W. OPQ: a MATLAB suite of programs for generating orthogonal polynomials and related quadrature rules. <https://www.cs.purdue.edu/archives/2002/wxg/codes/OPQ.html>. Accessed: 03.04.2017.
- [27] GAUTSCHI, W. *Orthogonal polynomials: computation and approximation*. Numerical Mathematics and Scientific Computation. Oxford University Press, New York, 2004. Oxford Science Publications.
- [28] GOVAERTS, W., KUZNETSOV, Y. A., AND MEIJER, H. G. MATCONT. Numerical bifurcation analysis toolbox in MATLAB. <https://sourceforge.net/projects/matcont/>. Accessed: 03.04.2017.
- [29] GURTIN, M. E., AND MACCAMY, R. C. Non-linear age-dependent population dynamics. *Arch. Rational Mech. Anal.* 54 (1974), 281–300.

- [30] GYLLENBERG, M. Stability of a nonlinear age-dependent population model containing a control variable. *SIAM J. Appl. Math.* 43, 6 (1983), 1418–1438.
- [31] GYLLENBERG, M. Mathematical aspects of physiologically structured populations: the contributions of J. A. J. Metz. *J. Biol. Dyn.* 1, 1 (2007), 3–44.
- [32] HALE, J. K., AND VERDUYN LUNEL, S. M. *Introduction to functional-differential equations*, vol. 99 of *Applied Mathematical Sciences*. Springer-Verlag, New York, 1993.
- [33] KERMACK, W. O., AND MCKENDRICK, A. G. A contribution to the mathematical theory of epidemics. *Proceedings of the Royal Society of London. Series A, Containing Papers of a Mathematical and Physical Character* 115, 772 (1927), 700–721.
- [34] KOOLJMAN, S. A. L. M., AND METZ, J. A. J. On the dynamics of chemically stressed populations: The deduction of population consequences from effects on individuals. *Hydrobiological Bulletin* 17, 1 (1983), 88–89.
- [35] LEUNG, K. Y., AND DIEKMANN, O. Dangerous connections: on binding site models of infectious disease dynamics. *J. Math. Biol.* 74, 3 (2017), 619–671.
- [36] MACDONALD, N. *Time lags in biological models*, vol. 27 of *Lecture Notes in Biomathematics*. Springer-Verlag, Berlin-New York, 1978.
- [37] MASTROIANNI, G., AND MILOVANOVIĆ, G. V. *Interpolation processes. Basic theory and applications*. Springer Monographs in Mathematics. Springer-Verlag, Berlin, 2008.
- [38] SHEN, J., TANG, T., AND WANG, L.-L. *Spectral methods. Algorithms, analysis and applications*, vol. 41 of *Springer Series in Computational Mathematics*. Springer, Heidelberg, 2011.
- [39] SHEN, J., AND WANG, L.-L. Some recent advances on spectral methods for unbounded domains. *Commun. Comput. Phys.* 5, 2-4 (2009), 195–241.
- [40] SZALAI, R. KNUT. <http://rs1909.github.io/knut/>. Accessed: 03.04.2017.
- [41] WANG, L.-L. Spectral methods. Algorithms, analysis and applications. <http://www.ntu.edu.sg/home/lilian/book.htm>, 2011. Accessed: 03.04.2017.
- [42] WEIDEMAN, J. A. C., AND REDDY, S. C. A MATLAB differentiation matrix suite. *ACM Trans. Math. Software* 26, 4 (2000), 465–519.
- [43] WELFERT, B. D. Generation of pseudospectral differentiation matrices. I. *SIAM J. Numer. Anal.* 34, 4 (1997), 1640–1657.

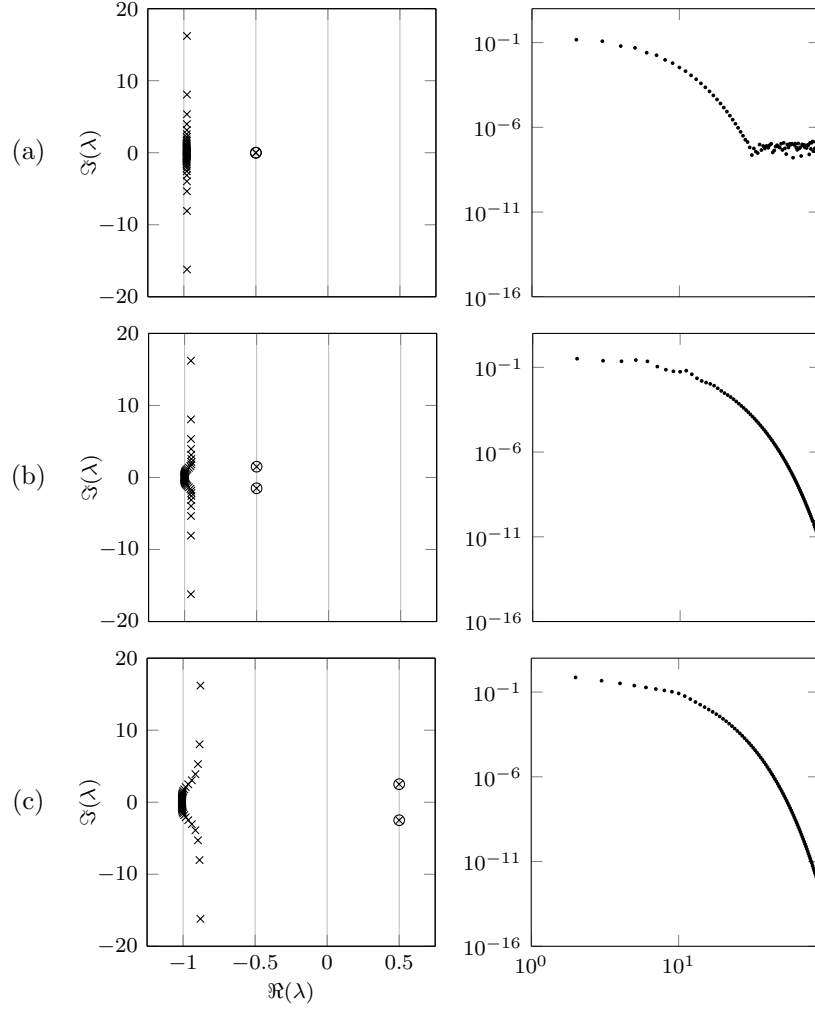


Figure 2: left: exact characteristic roots  $\lambda$  (25) (circles) and computed spectrum of  $\hat{A}_{50}$  (26) (crosses). Right: log-log plot of the absolute error in the approximation of the characteristic roots when increasing  $M$ . The set of parameter values are  $\mu = 2, \rho = 1$  and (a)  $a = 1, b_0 = -2.25$ , corresponding to  $\lambda = -0.5$ ; (b)  $a = 1, b_0 = -4.5$ , corresponding to  $\lambda = -0.5 \pm 1.5i$ ; (c)  $a = 3, b_0 = -12.5$ , corresponding to  $\lambda = 0.5 \pm 2.5i$ .

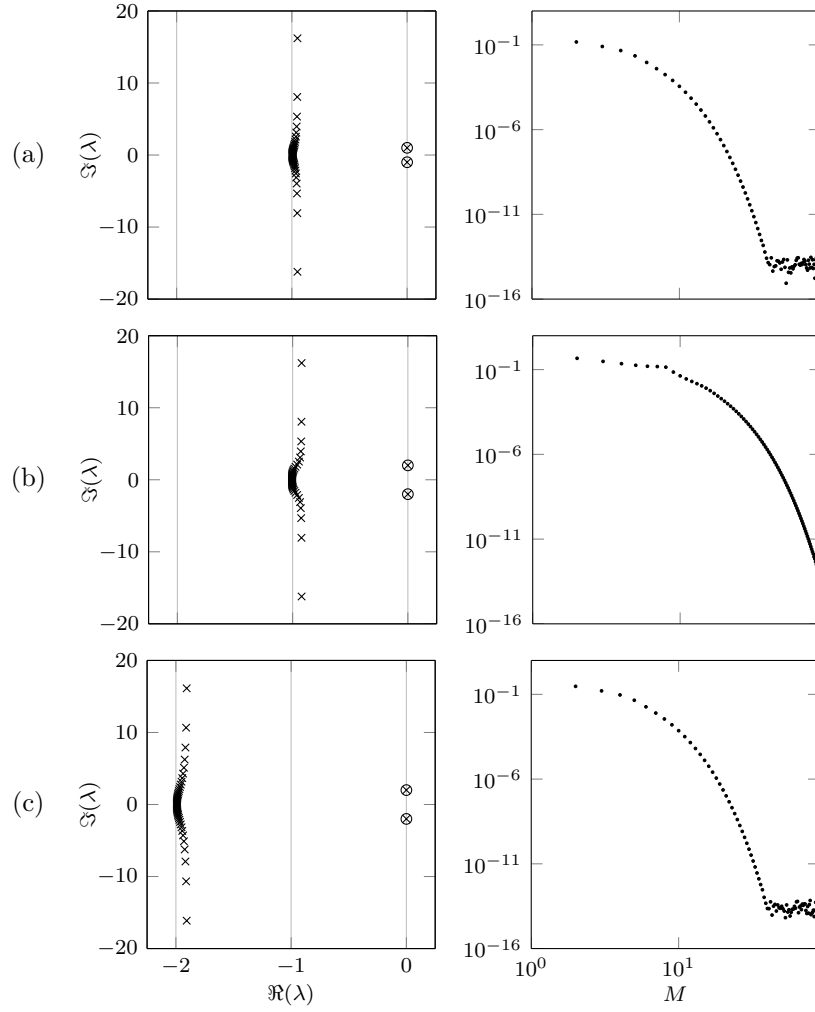


Figure 3: same as Figure 2, with parameter values (a)  $a = 2, b_0 = -5, \mu = 2, \rho = 1$ , corresponding to  $\lambda = \pm i$ ; (b)  $a = 2, b_0 = -8, \mu = 2, \rho = 1$ , corresponding to  $\lambda = \pm 2i$ ; (c)  $a = 4, b_0 = -20, \mu = 4, \rho = 2$ , corresponding to  $\lambda = \pm 2i$ .



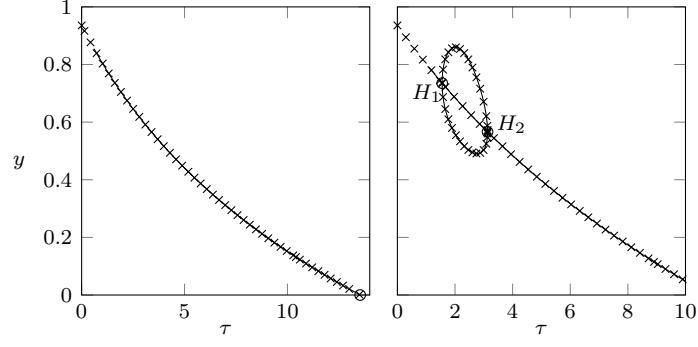


Figure 4: bifurcation diagram of  $y$  with respect to  $\tau$ , including the maximum and minimum value of the stable periodic orbit arising from the Hopf points, of the system of ODEs (28) (continuous line) and of the pseudospectral discretization of (27) with  $M = 10$  and  $\rho = (\delta_J + n/\tau)/4$  (crosses), with MATCONT tolerance  $\text{TOL} = 10^{-10}$  and model parameters  $\delta_A = 0.5$ ,  $\delta_J = 1$ ,  $a = 7$ ,  $b = 350$ , and (left)  $n = 5$ , (right)  $n = 7$ .

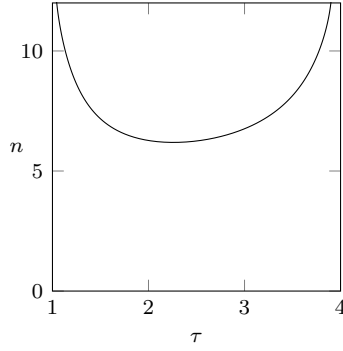


Figure 5: Hopf bifurcation curve in the parameter plane  $(\tau, n)$  computed from the pseudospectral discretization of (27), with parameters specified in the caption of Figure 4.

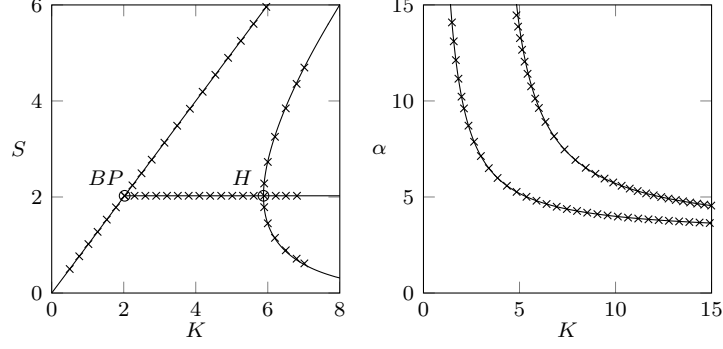


Figure 6: left: bifurcation diagram of  $S$  with respect to  $K$ , including the maximum and minimum value of the stable periodic orbit arising from the Hopf point, of the system of ODEs (30) (continuous line) and of the pseudospectral discretization of (29) with  $M = 20$  and  $\rho = \mu/2$  (crosses), with MATCONT tolerance  $TOL = 10^{-10}$  and model parameters  $\alpha = 10$ ,  $r = 3$ ,  $\mu = 1$ . Right: transcritical (lower curve) and Hopf (upper curve) bifurcation curves in the parameter plane  $(K, \alpha)$ .

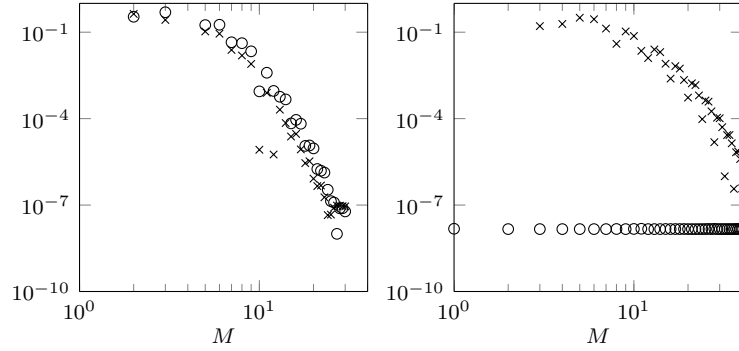


Figure 7: left: log-log plot of the absolute error between the Hopf bifurcation points  $\tau_1 \approx 1.55$  (crosses) and  $\tau_2 \approx 3.13$  (circles) computed from the system of ODEs (28) and the values obtained by pseudospectral discretization of (27), increasing the index  $M$ , with  $n = 7$  and the other parameters specified in the caption of Figure 4. Right: log-log plot of the absolute error between the transcritical bifurcation point  $K_{BP} \approx 2.02$  (circles) and the Hopf bifurcation point  $K_H \approx 5.88$  (crosses) computed from the system of ODEs (30) and the values obtained by pseudospectral discretization of (29), increasing the index  $M$ , with parameters specified in the caption of Figure 6.